energies

Article

Adaptive Online Extraction Method of Slot Harmonics for Multiphase Induction Motor

Jie Yu *, Youjun Zhang, Hongyuan Shen and Xiaoqin Zheng

College of Electrical Engineering, Qingdao University, Qingdao 266071, China
* Correspondence: yujie_ee@qdu.edu.cn

Abstract: The accurate extraction and analysis of slot harmonics caused by slotting in an induction motor are important for the motor's performance evaluation and state monitoring. However, the frequency distribution of rotor slot harmonics (RSHs) varies along with the operating states of the motor, such as motor speed and slip ratio, and the voltage and current signals of the motor only contain small-amplitude RSHs compared with other harmonics; both make it difficult to extract and analyze the RSHs accurately online. While offline extraction and filters with constant parameters are mainly utilized in available works, a novel adaptive extraction method for RSHs in a multiphase induction motor is proposed here to realize online RSH extraction under different speed and load conditions. In this paper, the RSHs in the multiphase induction motors are firstly modeled by using the magnetic potential permeability method, and the influence of a skewed rotor on RSHs is analyzed through a multisection method. Then, an adaptive extraction method of RSHs is proposed, which can effectively realize the online processing of RSHs of stator current. Finally, the experimental platform of a nine-phase induction motor has been used to verify the effectiveness of the proposed method under different speeds and load conditions, with a relative error of less than 1% in identifying the RSH frequency distribution.

Keywords: multiphase induction motor; rotor slot harmonics; adaptive filter; online identification

check for updates

Citation: Yu, J.; Zhang, Y.; Shen, H.; Zheng, X. Adaptive Online Extraction Method of Slot Harmonics for Multiphase Induction Motor. *Energies* **2022**, *15*, 6643. https://doi.org/10.3390/en15186643

Academic Editor: Anibal De Almeida

Received: 20 July 2022
Accepted: 2 September 2022
Published: 11 September 2022

Publisher's Note: MDPI stays neutral with regard to jurisdictional claims in published maps and institutional affiliations.

Copyright: © 2022 by the authors. Licensee MDPI, Basel, Switzerland. This article is an open access article distributed under the terms and conditions of the Creative Commons Attribution (CC BY) license (https://creativecommons.org/licenses/by/4.0/).

1. Introduction

Multiphase induction motors (IMs) have been widely used in electric transportation applications, such as electric vehicle drive, rail transport and ship propulsion [1]. Although the multiphase IM features a reliable structure, lower phase voltage level [2], convenience in maintenance [3] and good tolerant control capability [4,5], the working conditioning measurement is still vital for the healthy operation of IMs, in which the real-time extraction and analysis of voltage or current harmonics are important for providing essential or inherent information for motor control or monitoring.

On one hand, slot harmonics are generally regarded as disturbances for motor operation; they not only cause motor cost but also lead to torque ripples [6] and current fluctuation [7]. When the rotor is eccentric, the slot harmonic will also affect the magnetic pull force [8]. It is also necessary to optimize the stator and rotor slot number and slot dimensions of the motor within its design stage [9]. Fractional slot [10], closed-slot [11], skewed slot [12] and assisting magnetic pole [13] are all feasible methods for reducing slot harmonics, but the above methods cannot completely eliminate tooth harmonics. Therefore, slot harmonics need to be modeled and analyzed, which is usually combined with motor design and iron loss analysis [14] and efficiency estimation [15].

On the other hand, the time and frequency properties of slot harmonics are effective indicators that directly reveal the working condition of motor and can be used for fault detection, including broken rotor bar fault diagnosis [16] due to the irregular frequency distribution of rotor slot harmonics (RSHs), sensor-less rotor temperature estimation [17] by evaluating the rotor loss through RSHs, and the detection of stator winding faults [18], as well as the measurement of motor speed in real time because the slip ratio is inherently embedded in the frequencies of RSHs [19]. However, the modeling of slot harmonics cannot comprehensively consider the actual operating conditions such as temperature [20] and eccentric non-ideal conditions [21], as well as the other manufacturing errors [22], so the online extraction and analysis of motor slot harmonics are actually of priority before they can be further analyzed and utilized for the motor state monitoring and motor control methods. However, the motor tooth harmonics, especially the frequency distribution of RSHs, change with the motor running state, which makes it difficult to extract them online. In fact, the offline extraction and filters with constant parameters are mainly utilized in available works, which restricts the performance and accuracy of the online evaluation of RSH properties of induction motors.

In this paper, we introduce an adaptive rotor slot harmonic extraction algorithm for multiphase induction motors. The time and frequency properties of RSHs are firstly modeled and analyzed, especially under the transients of load or speed change. Then an adaptive online extraction and analysis method for RSHs is proposed to cope with the current harmonics of the motor in operation, especially for different speed and load conditions. Finally, a nine-phase induction motor platform was utilized to verify the proposed adaptive online extraction and analysis method for primary RSHs (PSHs).

2. The Model and Analysis of Rotor Slot Harmonics for Multiphase Induction Motors

2.1. The Analytical Model of RSHs for Multiphase IMs

The rotor slot harmonics are generated by the cogging effect and are difficult to completely eliminate by skewed slot and other methods. The open slot on the stator and rotor has a modulation effect on the air gap magnetic field, as shown in Figure 1, and is furtherly reflected in the motor voltage or current.

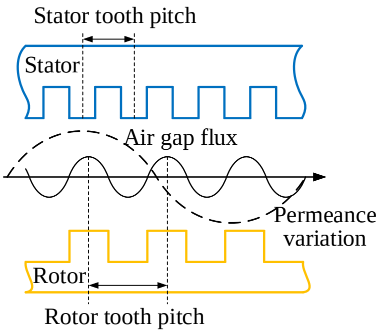

Figure 1. The cogging effect of motor slotting on air gap magnetic field.

To obtain the theoretical model of RSHs for multiphase IMs, the magnetic potential and permeability method is used here. For a multiphase induction motor in normal operation, its synthetic magnetic potential of stator and rotor windings is first listed as follows:

$$f(\theta,t) = f_0(\theta,t) + \sum_{\nu} f_\nu(\theta,t) + \sum_{\mu} f_\mu(\theta,t) \tag{1}$$

where θ is mechanical rotor position, t is the time, f_0 is the fundamental component, f_v is the vth magnetic potential of stator windings and f_μ is the μth magnetic potential of rotor windings.

$$\begin{aligned} f_0(\theta,t) &= F_0\cos(p\theta - \omega_1 t - \varphi_0) \\ f_\nu(\theta,t) &= F_\nu\cos(\nu\theta - \omega_v t - \varphi_v) \\ f_\mu(\theta,t) &= F_\mu\cos(\mu\theta - \omega_\mu t - \varphi_\mu) \end{aligned} \tag{2}$$

in which p is the pole pair. ω_1, ω_v and ω_μ and φ_1, φ_v and φ_μ are respectively the angular frequencies and phases of each component. F_0, F_v and F_μ are their magnetic potential amplitudes.

As an example, if the number of slots per pole per phase is an integer for a nine-phase induction motor, the harmonic number of stator windings is

$$\nu = (18k_1 + 1)p, \quad k_1 \pm 1,\ \pm 2,\ \ldots \tag{3}$$

If k_1 is an integral multiple of the number of slots per pole per phase q_1, such as $k_1 = \pm q_1, \pm 2q_1, \pm 3q_1 \ldots$, the order of stator slot harmonics will be obtained as

$$\nu_z = (18q_1k_1 + 1)p = k_1Z_1 + p \;\; k_1 = \pm 1, \pm 2, \cdots \tag{4}$$

where Z_1 is the stator slot number.

Then, the magnetic potential harmonic order for a squirrel-cage rotor winding can be defined as

$$\mu = k_2Z_2 + \nu \;\; k_2 = \pm 1, \pm 2, \cdots \tag{5}$$

where Z_2 is the rotor slot number.

Meanwhile, the fundamental magnetic field in the air gap will induce the electromotive force of rotor slot harmonics with the frequencies as

$$\mu_z = k_2Z_2 + p \;\; k_2 = \pm 1, \pm 2, \cdots \tag{6}$$

As the magnetic potential has been modeled, the characteristics of air gap permeance due to stator and rotor slots should also be analyzed. With slots on the stator and rotor, the air gap permeability can be approximately expressed as

$$\begin{aligned} \lambda(\theta, \mathrm{t}) &= \Lambda_0\Big(1 + \frac{\sum_{k1}\lambda_{k1}}{\Lambda_0}\Big)\Big(1 + \frac{\sum_{k2}\lambda_{k2}}{\Lambda_0}\Big) \\ &\approx \Lambda_0 + \sum_{k1}\lambda_{k1} + \sum_{k2}\lambda_{k2} + \sum_{k1}\sum_{k2}\lambda_{k1}\lambda_{k2} \end{aligned} \tag{7}$$

where Λ_0 is the constant or DC part, Λ_{k1} is the k_1th magnetic permeance harmonics only with stator slots, Λ_{k2} is the k_2th magnetic permeance harmonics only with rotor slots and $\Lambda_{k1}\Lambda_{k2}$ is due to the relative effect between stator and rotor slots.

$$\Lambda_0 = \frac{\mu_0}{\delta K_\mathrm{c}} \tag{8}$$

$$\Lambda_{k1} = -\Lambda_0(-1)^{k1}(K_{c1} - 1)\left|\frac{\sin k_1 \frac{K_{c1}-1}{K_{c1}}\pi}{k_1 \frac{K_{c1}-1}{K_{c1}}\pi}\right| \tag{9}$$

$$\Lambda_{k2} = -\Lambda_0(-1)^{k2}(K_{c2} - 1)\left|\frac{\sin k_2 \frac{K_{c2}-1}{K_{c2}}\pi}{k_2 \frac{K_{c2}-1}{K_{c2}}\pi}\right| \tag{10}$$

$$\lambda_{k1k2} = \frac{\Lambda_{k1}\Lambda_{k2}}{\Lambda_0}\cos[(\pm k_1Z_1 - k_2Z_2)\theta - k_2\frac{Z_2}{p}(1 - s)\omega t] \tag{11}$$

where δ is the nominal air gap length; K_c, K_{c1} and K_{c2} are the Karter coefficients, which are related to the dimensions of stator and rotor slots.

According to the properties of magnetic potential and permeance discussed above, the air gap flux distribution can be calculated as follows:

$$\begin{gathered} b(\theta,t)=f(\theta,t)\lambda(\theta,t) \\ =\left\{f_0(\theta,t)+\sum_{\nu} f_\nu(\theta,t)+\sum_{\mu} f_\mu(\theta,t)\right\}\cdot\left\{\Lambda_0+\sum_{k_1}\lambda_{k_1}+\sum_{k_2}\lambda_{k2}\right\} \\ \approx\left\{\begin{array}{c} F_0\Lambda_0\cos(p\theta-\omega_1 t-\varphi_0)+\sum_{\nu} F_\nu\Lambda_0\cos(\nu\theta-\omega_1 t-\varphi_1) \\ +\sum_{\mu} F_\mu\Lambda_0\cos(\mu\theta-\omega_\mu t-\varphi_2) \end{array}\right\} \\ +\left\{\sum_{k1}\frac{F_0\Lambda_{k1}}{2}\cos[(\pm k_1 Z_1+p)\theta-\omega_1 t-\varphi_0)]\right\} \\ +\left\{\sum_{k2}\frac{F_0\Lambda_{k2}}{2}\cos\left[(\pm k_2 Z_2+p)\theta-\left(\pm\frac{k_2 Z_2}{p}(1-s)+1\right)\omega_1 t-\varphi_0)\right]\right\} \end{gathered} \quad (12)$$

in which the $\Lambda_{k1}\Lambda_{k2}$ component is omitted for simplicity; s is the slip ratio. The rotor slot harmonics for windings is

$$\begin{gathered} b_{f\mu_z}(\theta,t)=\sum_{\mu_z} B_{f\mu_z}\cos(\mu_z\theta-\omega_\mu t-\varphi_2) \\ B_{f\mu_z}=F_{\mu_z}\Lambda_0=\frac{p}{\mu}K_\delta\frac{I_2'}{I_0}B_\delta \end{gathered} \quad (13)$$

and the rotor slot harmonics for magnetic permeance is

$$\begin{gathered} b_{\Lambda\mu_z}(\theta,t)=\sum_{\mu_z} B_{\Lambda\mu_z}\cos(\mu_z\theta-\omega_\mu t-\varphi_0) \\ B_{\Lambda\mu_z}=\frac{1}{2}\frac{F_0}{K_\delta}\Lambda_{k2}=\frac{1}{2}\frac{\Lambda_{k2}}{\Lambda_0}B_\delta \end{gathered} \quad (14)$$

where $\mu_z=k_2Z_2+pk_2=\pm1,\pm2,\cdots$

Taking the primary rotor slot harmonic (PSH) as an example, its time domain expression can be divided into two parts: the first one B_{r1} is generated by the fundamental magnetic potential of the motor, along with the magnetic conductivity due to slot cogging effect, and the other one B_{r2} is caused by the interaction between the RSH induced magnetic potential and the DC component of air gap magnetic conductivity. According to Equations (12)–(15), and by combining the components with the same frequency, the primary rotor slot harmonics (PSHs) can be modeled as follows:

$$\begin{aligned} B_r(\theta,t) &= B_{r1}(\theta,t)+B_{r2}(\theta,t) \\ &= (F_{r(Z_2/p-1)}\Lambda_0+\tfrac{1}{2}F_0\Lambda_r)\cos\left[(Z_2-p)\theta-\left(\tfrac{Z_2}{p}(1-s)-1\right)\omega_1 t\right] \\ &\quad+(F_{r(Z_2/p+1)}\Lambda_0+\tfrac{1}{2}F_0\Lambda_r)\cos\left[(Z_2+p)\theta-\left(\tfrac{Z_2}{p}(1-s)+1\right)\omega_1 t\right] \\ &= B_{rsh1}(\theta,t)+B_{rsh2}(\theta,t) \end{aligned} \quad (15)$$

where $B_{t1-}(\theta,t)$ and $B_{t1+}(\theta,t)$ are two side frequency components of PSH, $F_{r_{(Z_2/p-1)}}$ and $F_{r_{(2,p+1)}}$ are amplitudes of rotor cogging MMFs and Λ_r is the amplitude of sinusoidal air gap permeance due to rotor cogging effect.

The frequencies of PSH f_{t1-} and f_{t1+} are respectively

$$f_{t1-}=\left(\frac{Z_2}{p}(1-s)-1\right)f_1=(\frac{Z_2n}{60f_1}-1)f_1 \quad (16)$$

$$f_{t1+}=\left(\frac{Z_2}{p}(1-s)+1\right)f_1=(\frac{Z_2n}{60f_1}+1)f \quad (17)$$

in which f_1 is the frequency of the fundamental magnetic field.

It can be found from Equations (17) and (18) that the frequencies of primary rotor slot harmonics change along with the driving frequency of the inverter and inherently contain the information of slip ratio s, which is adjusted during motor operation dynamics, thus making it difficult to extract the RSHs online.

2.2. The Effect of Skewed Slot Rotor on PSHs

The skewed slot of the rotor can effectively reduce the PSHs, thus improving the cogging torque as well as the electromechanical vibration and noise for an operating motor. In the magnetic field analysis, the effect of skewed slot can be equivalent to the decrease in winding coefficient and influence the distribution of PSHs, thus then changing the phase of electric potential harmonic for PSHs, so that their amplitudes will decrease. In addition, the skewed slot rotor also weakens F_1.

Here we use a multisection method [23] to analyze the properties of PSHs with skewed rotor slots. In this method, the motor with a skewed slot rotor is segmented into several parts, and each motor part is regarded with no slot skewness. Then, the electromagnetic field of each motor part is calculated through the 2D finite element method [24], and the calculated results of each part are summed up and then averaged, so as to analyze the effect of rotor slot skewness.

The equivalent model of the multisection method mentioned above can be illustrated in Figure 2, where the motor with a skewed slot rotor is divided into K segments, with γ as the rotor slot slope. Thus, the rotor slot skewed angle between adjacent motor parts can be obtained as $\theta = \gamma/k$.

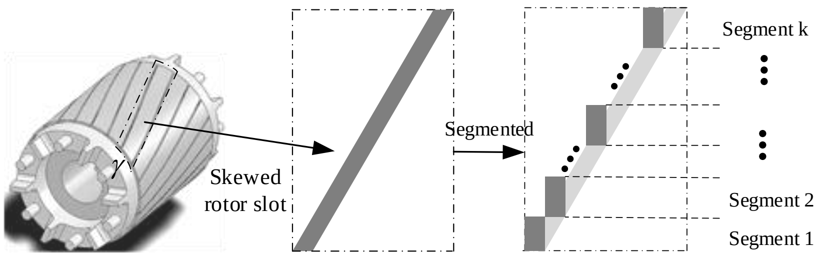

Figure 2. The equivalent multisegmented model for a skewed rotor slot.

By coping with the elements related to the vector magnetic potential in the finite element model of each motor segment, the finite element calculation model can be obtained. As an example, a nine-phase IM with its main parameters listed in Table 1 and the rotor slot skewed at a single stator pitch (5°) is divided into seven segments here. Each segment is regarded as a motor part without slot skewness and analyzed through FEA simulation. The 2D FEA simulation results of magnetic field distribution of a single segment are plotted in Figure 3.

Table 1. Main parameters of nine-phase induction motor platform.

Symbol	Parameter	Value
P_N	Rated motor power	8 kW
m	Phase number	9
f_N	Rated power supply frequency	50 Hz
P	Pole pairs	2
n_N	Rated speed	1477 r/min
U_N	Rated phase voltage	85 V
I_N	Rated phase current	12.87 A
Z_1	Stator slot number	72
Z_2	Rotor slot number	54
β	Pitch ratio	5/6

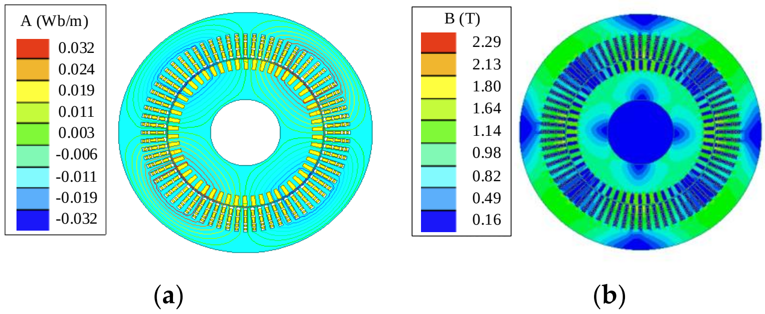

Figure 3. The 2D FEA simulation results of a segmented nine-phase IM: (**a**) the distribution of A (Wb/m); (**b**) the distribution of B (T).

After the 2D FEA simulation of each motor segment, the calculated results are further summed and averaged; the simulated amplitudes of PSH without and with the rotor slot skewness in stator induced phase voltage are shown in Figure 4.

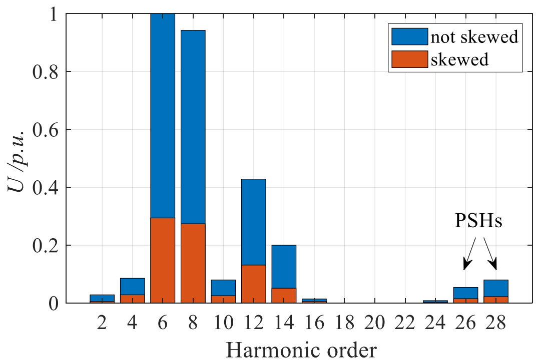

Figure 4. The effect of skewed rotor slot on the induced phase voltage harmonics of a nine-phase IM (p.u.).

It can be seen from Figure 4 that when the rotor slot is skewed by a stator tooth pitch, the amplitude of PSHs decreases significantly in stator induced phase voltage, compared with the non-skewed case. At the same time, the other harmonics are also reduced.

3. Adaptive Online Extraction of PSHs from Stator Currents

Because the rotor slot harmonic changes dynamically with the running state of the motor, and its amplitude is small and the signal−to−noise ratio is very low, it is actually difficult to use a filter with constant coefficients to realize the online extraction and analysis for these harmonics. Therefore, an adaptive filter is needed to process the stator current signal, so as to eliminate the unrequired harmonics but retain the PSH components.

3.1. The Online Parameter Updated Algorithm for the Adaptive Online Extraction Filter for PSHs

According to Equations (16) and (17), the center frequency of adaptive passband filter f_{pre0} and passband width f_{pw} are designed as

$$f_{pre0} = \frac{Z_2 f_1}{p},\ f_{pw} = 4f_1 \tag{18}$$

Therefore, the lower and upper angular cut-off frequencies are respectively

$$\omega_1 = \frac{4\pi(f_{pre0} - 2f_1)}{F_s},\ \omega_2 = \frac{4\pi(f_{pre0} + 2f_1)}{F_s} \tag{19}$$

A four-order Butterworth lowpass filter is then designed, with the transfer function of the Butterworth lowpass filter being

$$H_{LP}(s) = \frac{1}{s^4 + 2.6131259s^3 + 3.4142136s^2 + 2.6131259s + 1} \tag{20}$$

Then the digital IIR bandpass filter can be obtained through bilinear transform [25],

$$\begin{aligned} H_{BP}(z) &= H_{LP}(s)\big|_{s=D\frac{z^{-2}-Ez^{-1}+1}{1-z^{-2}}} \\ &= \frac{b_0+b_1z^{-1}+b_2z^{-1}+b_3z^{-3}}{a_0-a_1z^{-1}-a_2z^{-1}-a_3z^{-3}-a_4z^{-4}} \end{aligned} \tag{21}$$

where the coefficients of the filter can be obtained as

$$b_0 = \frac{1}{D^2+\sqrt{2}D+1},\ b_2 = \frac{-2}{D^2+\sqrt{2}D+1},\ b_1 = b_3 = 0 \tag{22}$$

$$\begin{aligned} a_0 = 1,\ a_1 &= \frac{-(2D^2E+\sqrt{2}DE)}{D^2+\sqrt{2}D+1},\ a_2 = \frac{D^2E^2+2D^2-2}{D^2+\sqrt{2}D+1}, \\ a_3 &= \frac{\sqrt{2}DE-2D^2E-2}{D^2+\sqrt{2}D+1},\ a_4 = \frac{D^2-\sqrt{2}D+1}{D^2+\sqrt{2}D+1} \end{aligned} \tag{23}$$

$$D = \cot\left(\frac{\omega_2-\omega_1}{2}\right),\ E = \frac{2\cos\left(\frac{\omega_2+\omega_1}{2}\right)}{\cos\left(\frac{\omega_2-\omega_1}{2}\right)} \tag{24}$$

Taking the direct type II transposed IIR filter as an example, the realization structure of the adaptive filter is shown in Figure 5, where K is the gain of the adaptive filter. The fundamental frequency track can be realized through phase-locked loop (PLL) or directly obtained from the inverter [26].

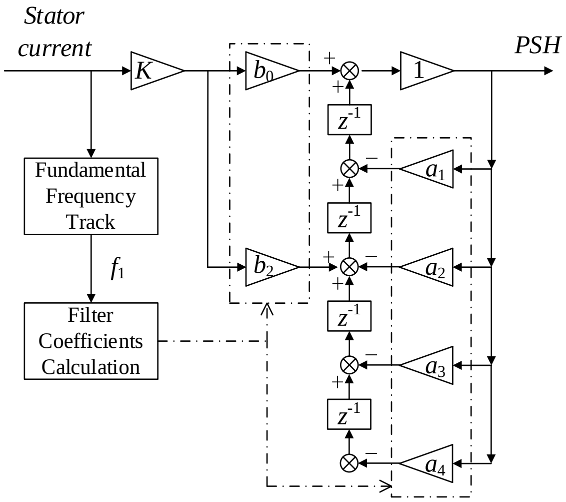

Figure 5. The diagram of the adaptive filter for PSH extraction.

3.2. The Online Frequency Identification of PSHs and Verification

As the disturbances have been eliminated from the output of the adaptive filter mentioned above, the signal-to-noise ratio of the PSH signal will be significantly enhanced and can be further utilized for further analysis.

Additional processing is still needed to accurately identify the frequency of PSH. FFT and phase-locked loop (PLL) are the commonly used methods for calculating signal frequency. Since the output signal of the adaptive extraction filter still contains multiple frequency components and their frequencies change in real time, the PLL method is not applicable here for achieving stable output. Therefore, the FFT algorithm is used in this paper to analyze the spectrum of the output signal of the adaptive filter. The complete processing algorithm is diagramed in Figure 6, in which the adaptive extraction filter has already been illustrated in Figure 4 in detail. The anti-aliasing processing, decimation and signal reconstruction are the standard pre-processing of the signal before the FFT. The signal reconstruction reuses the sampling points discarded in the process of decimation, so as to increase the total signal length and improve the frequency identification accuracy. The frequency verification assures that the identified frequencies of PSHs are reasonable; for example, the difference between f_{t1-} and f_{t1+} should be $2f_1$ under any working conditions.

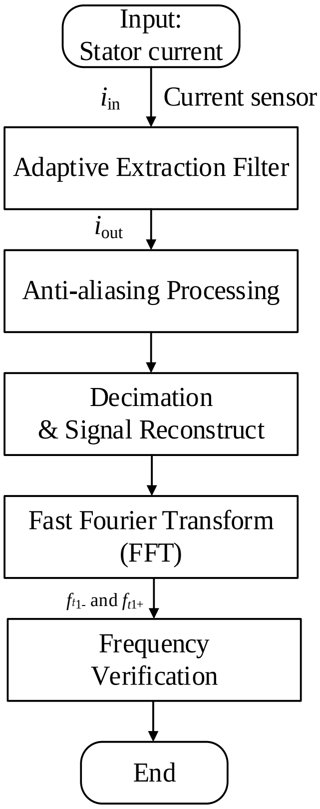

Figure 6. The online extraction and frequency identification of PSH.

The convergence rate is generally a critical concern of most adaptive filters due to the inherent signal feedback. However, the proposed online parameter update algorithm is a sequentially computed one, thus resulting in no convergence problem. Furthermore, the signal output transients due to filter parameter update will be averaged and diminished during the following FFT calculation and thus will not affect the RSH extraction results.

Another verification of the proposed method can be carried out by referring to actual motor speed. By combining Equations (17) and (18), the relationship between the frequency of PSHs and motor speed can be obtained as

$$f_{t1-} + f_{t1+} = \frac{Z_2 n}{15p} \tag{25}$$

4. Experimental Results

4.1. Experiment Platform Setup

A nine-phase induction motor platform, as shown in Figure 7, was established to verify the proposed adaptive online extraction and analysis method for PSHs. In this platform, a nine-phase squirrel-cage induction motor is driven by a multiphase inverter. The induction motor is coaxially connected to a DC generator, which is excited by a Siemens SINAMICS DCM regulator and serves for load adjustment. Speed and torque sensors are also installed with accuracies of 0.1 N·m and 1 r/min.

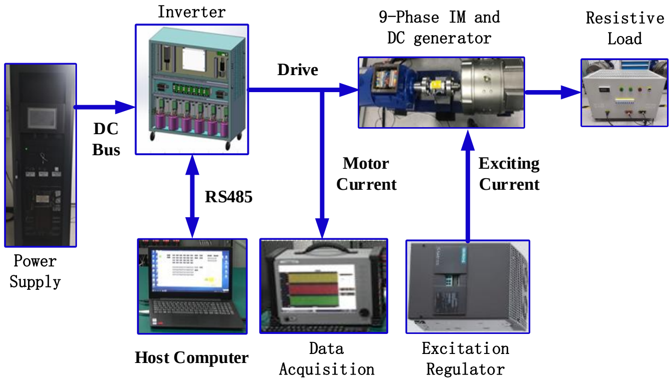

Figure 7. The nine-phase induction motor platform.

The stator current is measured through an LEM LA-25P current sensor and then A/D converted by ADS1203 and anti-aliasing processed by Xilinx xc4vlx25 FPGA at 10MHz rate before it is obtained by TI TMS320F28335 DSP. Differential signal measurement and Sigma-Delta ADC sample are utilized to improve the SNR. All the main parameters of the platform are listed in Table 1.

4.2. The PSH Extraction Results

Based on the above experimental device, the PSH characteristics of the motor were extracted under different rotational speeds and loads by utilizing the proposed adaptive online filter. In order to compare and analyze the time domain and frequency domain characteristics of the stator current and PSH of the nine-phase induction motor before and after adaptive filtering, The comparisons of the input and output of the adaptive PSH filter in time and frequency domain are given under different working conditions of speed 239–1396 rpm and torque 4.9–16.5 N·m, as shown in Figures 8–15. It can be found that the proposed filter can effectively extract the PSHs from the stator current signal, which is rich in harmonics. All the above extraction and analysis results are summarized in Table 2.

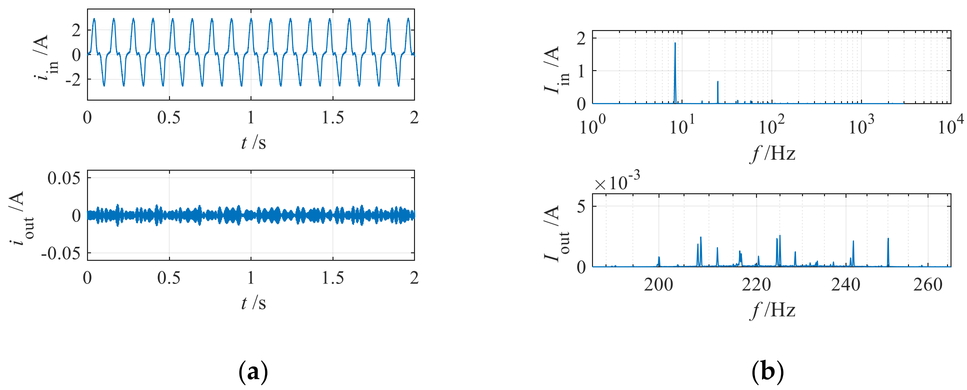

Figure 8. The comparison of the input and output of adaptive PSH filter in time and frequency domain (239 r/min, T_L = 5.2 N·m): (**a**) time domain waveform; (**b**) frequency distribution.

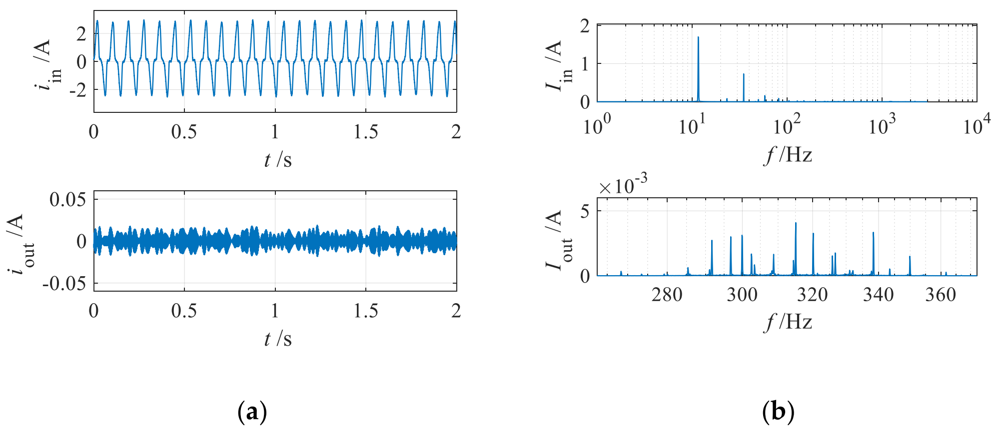

Figure 9. The comparison of the input and output of adaptive PSH filter in time and frequency domain (342 r/min, T_L = 4.9 N·m): (**a**) time domain waveform; (**b**) frequency distribution.

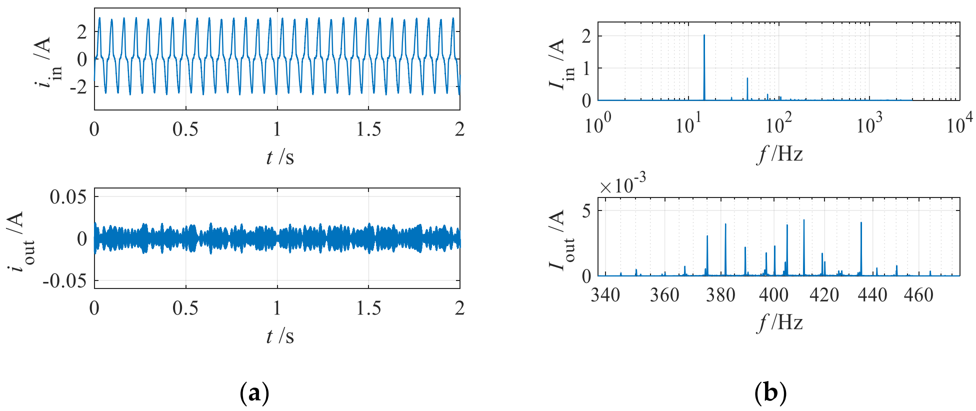

Figure 10. The comparison of the input and output of adaptive PSH filter in time and frequency domain (440 r/min, T_L = 6.0 N·m): (**a**) time domain waveform; (**b**) frequency distribution.

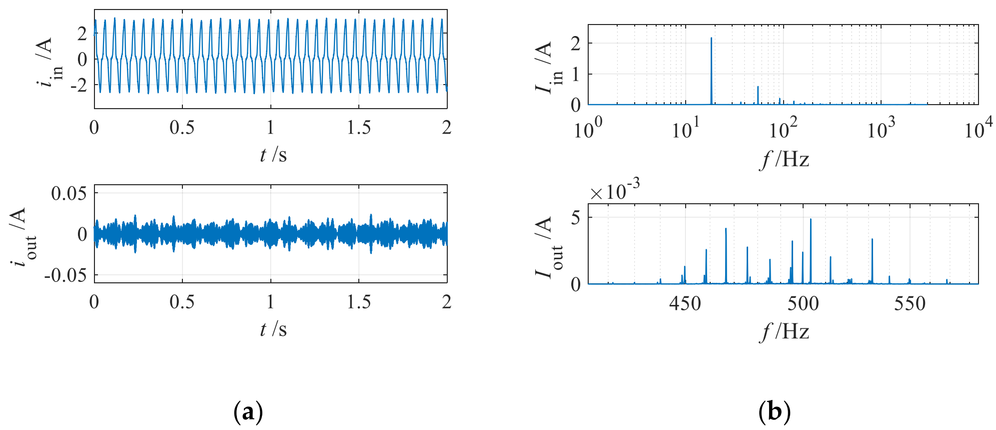

Figure 11. The comparison of the input and output of adaptive PSH filter in time and frequency domain (538 r/min, T_L = 7.0 N·m): (**a**) time domain waveform; (**b**) frequency distribution.

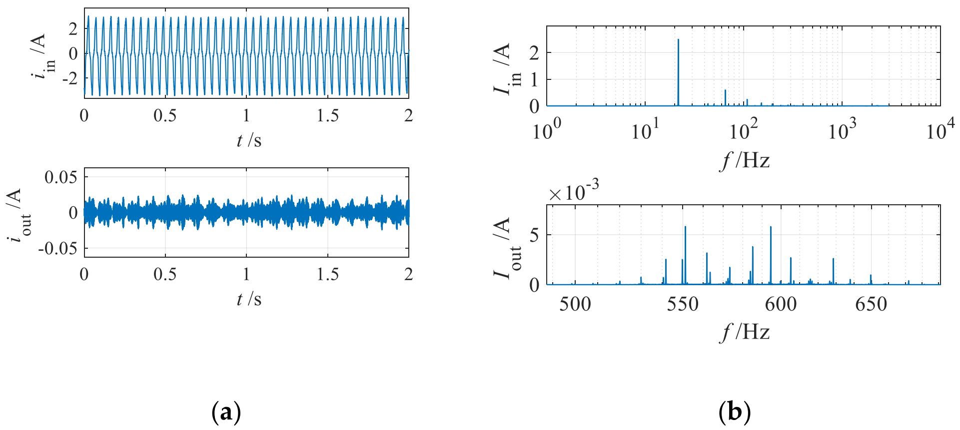

Figure 12. The comparison of the input and output of adaptive PSH filter in time and frequency domain (636 r/min, T_L = 8.3 N·m): (**a**) time domain waveform; (**b**) frequency distribution.

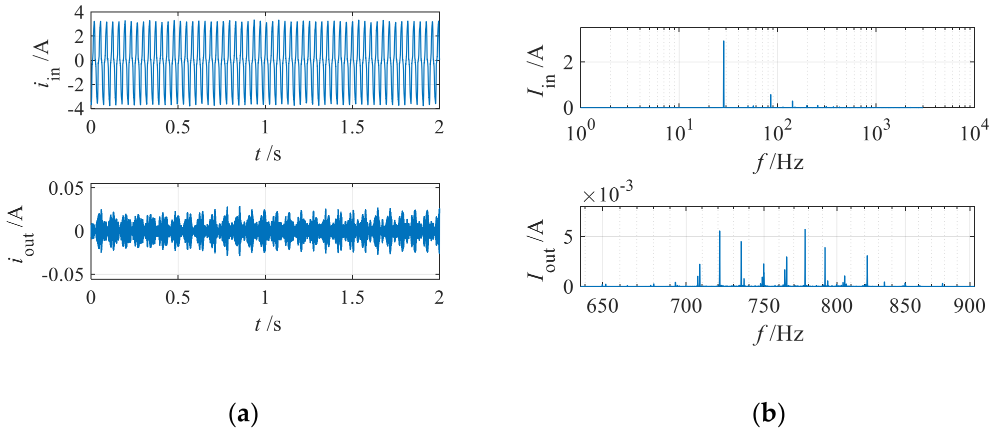

Figure 13. The comparison of the input and output of adaptive PSH filter in time and frequency domain (832 r/min, T_L = 10.5 N·m): (**a**) time domain waveform; (**b**) frequency distribution.

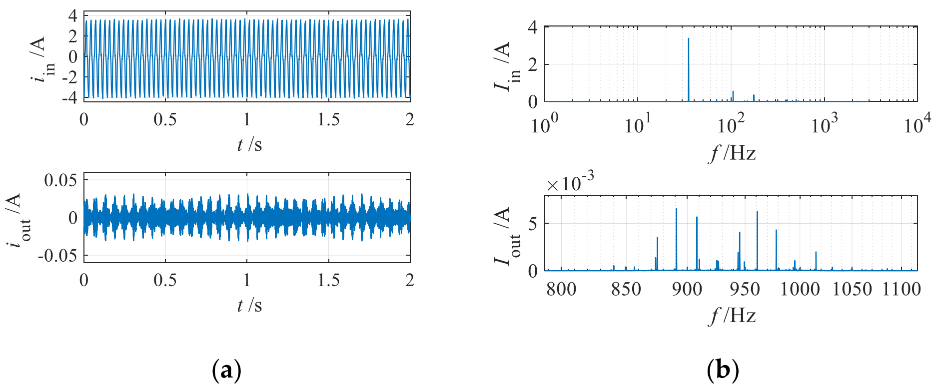

Figure 14. The comparison of the input and output of adaptive PSH filter in time and frequency domain (1028 r/min, T_L = 12.7 N·m): (**a**) time domain waveform; (**b**) frequency distribution.

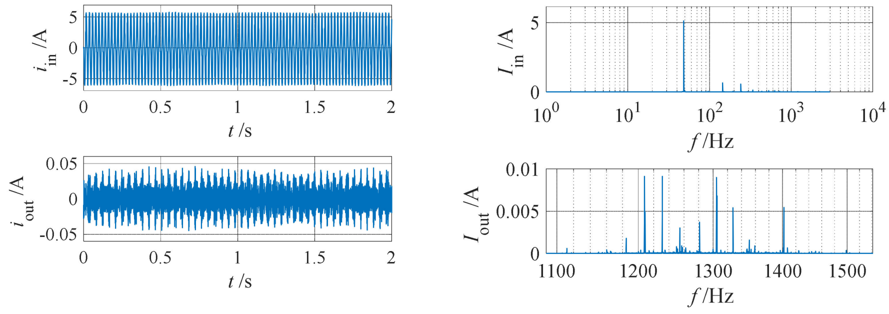

(**a**) (**b**)

Figure 15. The comparison of the input and output of adaptive PSH filter in time and frequency domain (1396 r/min, T_L = 16.5 N·m): (**a**) time domain waveform; (**b**) frequency distribution.

Table 2. The frequency distribution of PSHs under different speed and load conditions.

Speed n (rpm)	Torque (N·m)	f_1 (Hz)	f_{t1-} (Hz)	f_{t1+} (Hz)
239	5.2	8.3	208.4	225.1
342	4.9	11.7	296.8	320.2
440	6.0	15.0	381.7	411.7
538	7.0	18.3	466.6	503.3
636	8.3	21.6	551.2	594.6
832	10.5	28.3	721.1	777.8
1028	12.7	35.0	891.0	961.0
1396	16.5	48.3	1208.0	1304.6

4.3. Verification and Errors

The key metric of the proposed method is its universal applicability under different motor conditions. Compared with the available RSH extraction method that is designed for a certain motor speed and load condition, the proposed method is adjustable for different speed and load conditions with only one adaptive filter, which contributes to the scene working convenience. To better evaluate the accuracy of the proposed extraction method, the analytical model illustrated as Equation (25) is utilized with measured motor speeds at different working conditions. As the motor speeds can be easily measured online with enough accuracy through the resolvers or encoders, the proposed method can be more directly and effectively evaluated. The verification results are listed in Table 3, which shows that the errors of PSH extraction and frequency analysis are less than 1% for all tested working conditions. The error tends to increase with the decrease in speed. This is mainly because the PSHs are concentrated in the low-frequency domain and are close to each other at a low speed, which makes the extraction and analysis much more difficult. In fact, when the rotational speed continues to decrease, the bandwidth of the adaptive filter proposed is too narrow, which easily makes the output of the IIR filter oscillate or become unstable, making the extraction process invalid.

Table 3. Verification and errors.

Speed n (rpm)	Torque (N·m)	$Z_2n/15p$ (Hz)	$f_{t1-} + f_{t1-}$ (Hz)	*Relative Error (%)*
239	5.2	430.2	433.5	0.77
342	4.9	615.6	617.0	0.23
440	6.0	792.0	793.4	0.18
538	7.0	968.4	969.9	0.15
636	8.3	1144.8	1145.8	0.09
832	10.5	1497.6	1498.9	0.09
1028	12.7	1850.4	1852.0	0.09
1396	16.5	2512.8	2512.6	0.01

5. Conclusions

In this paper, an analytical model of PSHs was utilized to update the coefficients of an adaptive filter so that the PSHs of multiphase IMs could be extracted from a harmonic-rich motor current and analyzed online. It has been validated through experiments that the proposed method can be effectively utilized to cope with the changing frequency distribution of PSHs under different speed and load conditions.

The accuracy of RSH frequency identification has also been verified by referring to the measured rotor speed, with the relative error smaller than 1% in a wide speed range of 239–1396 rpm. In this case, the online-extracted properties of RSHs can be further utilized for motor cost and torque ripple evaluation and monitoring. However, further investigations are still needed for online extraction and analysis of RSHs at the ultra-low speed condition, since the passband of the IIR filter will be too narrow to be implemented.

Based on the proposed adaptive online extraction method, more RSH-related studies for multiphase induction motors, such as studies involving speed estimation, fault detection and state monitoring.

Author Contributions: Conceptualization, J.Y. and X.Z.; methodology, J.Y. and Y.Z.; software, H.S.; validation, J.Y. and H.S.; writing—original draft preparation, J.Y. and Y.Z.; writing—review and editing, J.Y. and Y.Z.; funding acquisition, J.Y. All authors have read and agreed to the published version of the manuscript.

Funding: Natural Science Foundation of Shandong Province (Grant No. ZR2021QE118), Key Project of Innovative Teaching Laboratory of Qingdao University in 2020 (Grant No. CXSYZD202001) and National College Students Innovation and Entrepreneurship Training Program of China (Grant No. S202011065023).

Institutional Review Board Statement: Not applicable.

Informed Consent Statement: Not applicable.

Data Availability Statement: The data used in this study are available from the authors upon reasonable request.

Conflicts of Interest: The authors declare no conflict of interest.

References

1. Levi, E. Multiphase Electric Machines for Variable-Speed Applications. *IEEE Trans. Ind. Electron.* **2008**, *55*, 1893–1909. [CrossRef]
2. Wang, H.; Wu, X.; Zheng, X.; Yuan, X. Virtual Voltage Vector based Model Predictive Control for a Nine-phase Open-end Winding PMSM with a Common DC bus. *IEEE Trans. Ind. Electron.* **2022**, *69*, 5386–5397. [CrossRef]
3. You, R.; Lu, X. Voltage Unbalance Compensation in Distribution Feeders using Soft Open Points. *J. Mod. Power Syst. Clean Energy* **2022**, *10*, 1000–1008. [CrossRef]
4. Gonzalez-Prieto, A.; Aciego, J.J.; Gonzalez-Prieto, I.; Duran, M.J. Automatic Fault-Tolerant Control of Multiphase Induction Machines: A Game Changer. *Electronics* **2020**, *9*, 938. [CrossRef]
5. Kellner, J.; Kaščák, S.; Ferková, Ž. Investigation of the Properties of a Five-Phase Induction Motor in the Introduction of New Fault-Tolerant Control. *Appl. Sci.* **2022**, *12*, 2249. [CrossRef]
6. Li, X.; Xue, Z.; Zhang, L.; Hua, W. A low-complexity three-vector-based model predictive torque control for SPMSM. *IEEE Trans. Power Electron.* **2021**, *36*, 13002–13012. [CrossRef]
7. Joksimović, G.; Levi, E.; Kajević, A.; Mezzarobba, M.; Tessarolo, A. Optimal Selection of Rotor Bar Number for Minimizing Torque and Current Pulsations Due to Rotor Slot Harmonics in Three-Phase Cage Induction Motors. *IEEE Access* **2020**, *8*, 228572–228585. [CrossRef]
8. Frauman, P.; Burakov, A.; Arkkio, A. Effects of the Slot Harmonics on the Unbalanced Magnetic Pull in an Induction Motor with an Eccentric Rotor. *IEEE Trans. Magn.* **2007**, *43*, 3441–3444. [CrossRef]
9. Bień, A.; Drabek, T.; Kara, D.; Kołacz, T. Reduction in the Cogging Torques in the DCEFSM Motor by Changing the Geometry of the Rotor Teeth. *Energies* **2022**, *15*, 2455. [CrossRef]
10. Guo, L.; Xu, J.; Wu, S.; Xie, X.; Wang, H. Analysis and Design of Dual Three-Phase Fractional-Slot Permanent Magnet Motor with Low Space Harmonic. *IEEE Trans. Magn.* **2022**, *58*, 8100112. [CrossRef]
11. Zhou, G.; Shen, J. Current Harmonics in Induction Machine with Closed-Slot Rotor. *IEEE Trans. Ind. Appl.* **2017**, *53*, 134–142. [CrossRef]

12. Asad, B.; Vaimann, T.; Belahcen, A.; Kallaste, A.; Rassolkin, A.; Van Khang, H.; Ghahfarokhi, P.S.; Naseer, M.U.; Iqbal, M.N. The Modeling and Investigation of Slot Skews and Supply Imbalance on the Development of Principal Slotting Harmonics in Squirrel Cage Induction Machines. *IEEE Access* **2021**, *9*, 165932–165946. [CrossRef]
13. Chen, Q.; Xu, G.; Liu, G.; Zhai, F.; Eduku, S. Reduction of Torque Ripple Caused by Slot Harmonics in FSCW Spoke-Type FPM Motors by Assisted Poles. *IEEE Trans. Ind. Electron.* **2020**, *67*, 9613–9622. [CrossRef]
14. Zhang, D.; Liu, T.; Zhao, H.; Wu, T. An Analytical Iron Loss Calculation Model of Inverter-Fed Induction Motors Considering Supply and Slot Harmonics. *IEEE Trans. Ind. Electron.* **2019**, *66*, 9194–9204. [CrossRef]
15. Diarra, M.N.; Yao, Y.; Li, Z.; Niasse, M.; Li, Y.; Zhao, H. In-Situ Efficiency Estimation of Induction Motors Based on Quantum Particle Swarm Optimization-Trust Region Algorithm (QPSO-TRA). *Energies* **2022**, *15*, 4905. [CrossRef]
16. Benouzza, N.; Boudinar, A.H.; Bendiabdellah, A.; Khodja, M. Slot harmonic frequency detection as a technique to improve stator current spectrum approach for broken rotor bars fault diagnosis. In Proceedings of the 2015 Intl Aegean Conference on Electrical Machines & Power Electronics (ACEMP), 2015 Intl Conference on Optimization of Electrical & Electronic Equipment (OPTIM) & 2015 Intl Symposium on Advanced Electromechanical Motion Systems (ELECTROMOTION), Side, Turkey, 2–4 September 2015; pp. 118–122. [CrossRef]
17. Gao, Z.; Habetler, T.G.; Harley, R.G.; Colby, R.S. A Sensorless Rotor Temperature Estimator for Induction Machines Based on a Current Harmonic Spectral Estimation Scheme. *IEEE Trans. Ind. Electron.* **2008**, *55*, 407–416. [CrossRef]
18. Ray, S.; Dey, D. Development of a Comprehensive Analytical Model of Induction Motor under Stator Intern Turn Faults Incorporating Rotor Slot Harmonics. *IEEE Trans. Ind. Electron.* **2022**. [CrossRef]
19. Degner, M.W.; Lorenz, R.D. Position estimation in induction machines utilizing rotor bar slot harmonics and carrier-frequency signal injection. *IEEE Trans. Ind. Appl.* **2000**, *36*, 736–742. [CrossRef]
20. Duan, X.; Zhang, X.; Tang, Y.; Hao, M. Cogging Torque Reduction in PMSM in Wide Temperature Range by Response Surface Methodology. *Symmetry* **2021**, *13*, 1877. [CrossRef]
21. Park, J.-C.; Park, S.-H.; Kim, J.-H.; Lee, S.-G.; Lee, G.-H.; Lim, M.-S. Diagnosis and Robust Design Optimization of SPMSM Considering Back EMF and Cogging Torque due to Static Eccentricity. *Energies* **2021**, *14*, 2900. [CrossRef]
22. Lee, C.-S.; Kim, H.-J. Harmonic Order Analysis of Cogging Torque for Interior Permanent Magnet Synchronous Motor Considering Manufacturing Disturbances. *Energies* **2022**, *15*, 2428. [CrossRef]
23. Brescia, E.; Costantino, D.; Massenio, P.R.; Monopoli, V.G.; Cupertino, F.; Cascella, G.L. A Design Method for the Cogging Torque Minimization of Permanent Magnet Machines with a Segmented Stator Core Based on ANN Surrogate Models. *Energies* **2021**, *14*, 1880. [CrossRef]
24. Palangar, M.F.; Mahmoudi, A.; Kahourzade, S.; Soong, W.L. Electromagnetic and Thermal Analysis of a Line-Start Permanent-Magnet Synchronous Motor. In Proceedings of the 2020 IEEE Energy Conversion Congress and Exposition (ECCE), Detroit, MI, USA, 11–15 October 2020; pp. 502–508. [CrossRef]
25. Yu, J.; Zhu, C.; Wu, X. The Analysis of Displacement Estimation Errors of Demodulation Type Self-sensing Active Magnetic Bearings. *Proc. Chin. Soc. Electron. Eng.* **2019**, *10*, 5876–5884. [CrossRef]
26. Wang, H.; Zheng, X.; Yuan, X.; Wu, X. Low-Complexity Model-Predictive Control for a Nine-Phase Open-End Winding PMSM with Dead-Time Compensation. *IEEE Trans. Ind. Electron.* **2022**, *37*, 8895–8908. [CrossRef]